AIAA JOURNAL
Vol. 39, No. 8, August 2001

Stability and Strength of Composite Skew Plates Under Thermomechanical Loads

Maloy K. Singha,* L. S. Ramachandra,† and J. N. Bandyopadhyay‡
Indian Institute of Technology, Kharagpur 721 302, India

The buckling and postbuckling analysis of shear deformable composite skew plates subjected to combined uniaxial compression and uniform temperature rise has been carried out using the finite element method. The governing nonlinear finite element equation is posed as a sequence of linear eigenvalue problems, and each one of them is solved for different amplitudes of deflection to trace the thermal postbuckling path. A maximum strength criterion is used to identify the laminates that have failed in strength, and appropriate modifications are made to the stiffness matrix. The first-ply failure of laminates has also been predicted by Tsai–Hill and Tsai–Wu criteria. Postbuckling paths are traced for different boundary conditions of the plate. Specific numerical studies have been reported showing the effects of skew angle, initial uniaxial compression, and thickness-to-span ratio on the thermal postbuckling behavior of the eight-layered [45/− 45/0/90 deg]$_s$ symmetric plate. The presence of secondary instability has been identified while tracing the postbuckling path.

Nomenclature

a, b	=	dimensions of plate in x and y directions
E_L, E_T	=	Young's modulus in fiber and transverse to fiber directions
$\{F\}$	=	load vector
$G_{LT}, G_{LZ}\, G_{TZ}$	=	shear modulus
$(\boldsymbol{g}_1, \boldsymbol{g}_2, \boldsymbol{g}_3)$	=	covariant base vectors
$({}^1\boldsymbol{g}, {}^2\boldsymbol{g}, {}^3\boldsymbol{g})$	=	contravariant base vectors
h	=	thickness of plate
$[K_S]$, $[K_{\mathrm{nl}}]$, and $[K_g]$	=	linear, nonlinear, and geometric stiffness matrix, respectively
$[Q_{ij}]$	=	transformed reduced stiffness matrix
R, S, T	=	shear strengths of laminate
$({}^1r, {}^2r, {}^3r)$	=	contravariant components of position vector $\boldsymbol{r}$
T_{cr}	=	critical buckling temperature of plate, $^\circ C$
u_1^0, u_2^0, u_3^0	=	midsurface displacement of the plate in ${}^1r$, ${}^2r$, and ${}^3r$ directions, respectively
$u_{3,1}, u_{3,2}$	=	slope of plate in $\boldsymbol{g}_1$ and $\boldsymbol{g}_2$ directions, respectively
$u_{3,11}, u_{3,12}, u_{3,22}$	=	second derivatives of u_3 with respect to ${}^1r$ and ${}^2r$
X_T, X_C	=	tensile and compressive strength of laminate in fiber direction
Y_T, Y_C	=	tensile and compressive strength of laminate in transverse to fiber direction, respectively
$\{\alpha\}$	=	thermal expansion coefficient
γ_1, γ_2	=	rotation due to shear in $\boldsymbol{g}_1$ and $\boldsymbol{g}_2$ directions, respectively
$\{\delta\}$	=	global displacement vector
ε_{ij}	=	covariant components of strain tensor ε
${}^c\varepsilon_{ij}$ and ${}^c\sigma_{ij}$	=	strain and stress components in rectangular Cartesian coordinates
σ^{ij}	=	contravariant components of stress tensor σ

Received 28 March 2000; revision received 21 February 2001; accepted for publication 21 February 2001.

*Research Scholar, Department of Civil Engineering.
†Assistant Professor, Department of Civil Engineering.
‡Professor, Department of Civil Engineering.

Introduction

THE development of high-strength composite materials has revolutionized the concept of structural design. Today, fiber-reinforced composites are being widely used in aerospace, defense, and high-performance application areas based on their properties such as high strength, high stiffness-to-weight ratio, and the ease with which they can be tailored to any shape. At high temperatures, composite plates are found to buckle without the application of mechanical loads. Hence, the buckling and postbuckling strengths of composite plates have to be understood before they find extensive application.

Many researchers worked on the thermal buckling of rectangular plates. In the early works, the Rayleigh–Ritz method was used to obtain the critical temperature of plates.[1–4] Whitney and Ashton[5] studied the thermal buckling of composite plates using energy formulation. Many others[6–9] obtained the buckling temperature within the framework of finite element method. Huang and Tauchert[10] employed the finite element method to investigate the large deflection behaviors of flat, cylindrical, and doubly curved laminated panels. Singh et al.[11] studied the behavior of rectangular laminated composite plates under thermal loads. They used a c^1 continuous four-noded element to trace the postbuckling paths of the plate. Chen and Chen[12] obtained the thermal postbuckling paths for simply supported and clamped composite plates assuming linear variation of mechanical and thermal properties. Shen[13] used a perturbation technique to determine the buckling loads and postbuckling equilibrium paths of a simply supported perfect and imperfect composite plate subjected to combined axial and thermal load. Different computational models that are being used for the analysis of high-temperature multilayered composite plates and shells are reviewed critically by Noor and Burton[14] in a review paper.

However, the thermal buckling and postbuckling analysis of composite skew plates, which has applications in the construction of modern swept-wing aircraft and missiles, have received less attention from researchers. Prabhu and Durvasula[15] used Galerkin's method to study the thermal buckling behavior of an isotropic skew plate. Subsequently, Prabhu and Durvasula[16] studied the postbuckling behavior of clamped isotropic skew plates. A perturbation method was employed to obtain a set of linear partial differential equations, the solution of which was obtained using Galerkin's method. However, to the authors' knowledge, no work has been reported in the literature on the thermal buckling and postbuckling analysis of composite skew plates. Moreover, earlier research was confined to the buckling and postbuckling aspects only, without any attention to strength criteria, which is essential from the practical point of view.

In the present work, the postbuckling analysis of shear-deformable composite skew plates with immovable longitudinal

edges, subjected to combined uniaxial compression and uniform temperature rise, is carried out using the finite element method. A four-noded shear-deformable plate bending element is developed to discretize the plate. The nonlinear finite element equations are solved as a series of linear eigenvalue problems. A maximum strength criterion is used to identify the laminates that have failed in strength, and appropriate modifications are made to the stiffness matrix. For a particular case, the first-ply failure temperature evaluated on the basis of a maximum strength criterion has been compared with the failure temperature calculated using Tsai–Hill and Tsai–Wu criteria. The effects of skew angle, initial uniaxial compression, and thickness-to-span ratio on the critical buckling temperature and postbuckling behavior are studied. Thermal postbuckling paths are presented in the form of graphs for a specific eight-layered $[45/-45/0/90\ \text{deg}]_s$ composite plate. The material properties are assumed to be independent of temperature.

Finite Element Formulation

Figure 1a shows the rectangular Cartesian coordinate system along with the associated covariant base vectors $(\boldsymbol{g}_1, \boldsymbol{g}_2, \boldsymbol{g}_3)$ and contravariant base vectors $({}^1\boldsymbol{g}, {}^2\boldsymbol{g}, {}^3\boldsymbol{g})$ for the skew plate. Figure 1b represents the skew plate under initial uniaxial compressive load P. In Fig. 1a, ψ is the skew angle and a and b are the length and width of the plate; $(\boldsymbol{g}_1, \boldsymbol{g}_2, \boldsymbol{g}_3)$ and $({}^1\boldsymbol{g}, {}^2\boldsymbol{g}, {}^3\boldsymbol{g})$ are related to the rectangular Cartesian unit base vectors $(\boldsymbol{e}_1, \boldsymbol{e}_2, \boldsymbol{e}_3)$ by

$$\boldsymbol{g}_1 = \boldsymbol{e}_1, \qquad \boldsymbol{g}_2 = (\sin\psi)\boldsymbol{e}_1 + (\cos\psi)\boldsymbol{e}_2, \qquad \boldsymbol{g}_3 = \boldsymbol{e}_3$$

$${}^1\boldsymbol{g} = \boldsymbol{e}_1 - (\tan\psi)\boldsymbol{e}_2, \qquad {}^2\boldsymbol{g} = (\sec\psi)\boldsymbol{e}_2, \qquad {}^3\boldsymbol{g} = \boldsymbol{e}_3 \tag{1}$$

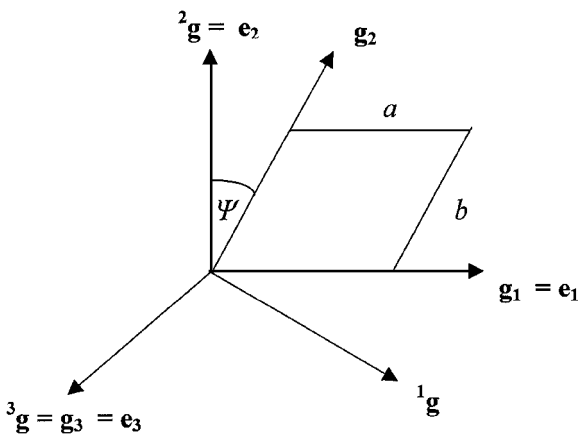

Fig. 1a Oblique coordinate system for skew plate.

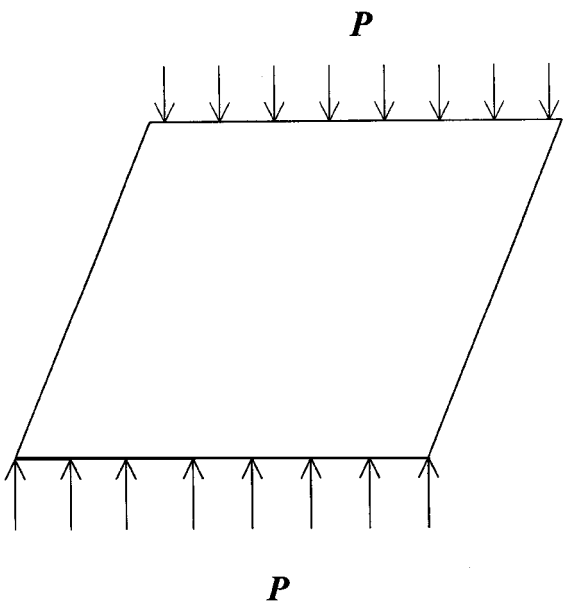

Fig. 1b Skew plate under initial uniaxial compression.

The covariant components of the displacement vector $\boldsymbol{u}$ $(\boldsymbol{u} = u_1{}^1\boldsymbol{g} + u_2{}^2\boldsymbol{g} + u_3{}^3\boldsymbol{g})$ of a shear deformable plate can be expressed[17,18] in terms of ${}^1r$, ${}^2r$, and ${}^3r$ as

$$u_1({}^1r, {}^2r, {}^3r) = u_1^0({}^1r, {}^2r) + {}^3r\,{}^1\phi({}^1r, {}^2r)$$

$$u_2({}^1r, {}^2r, {}^3r) = u_2^0({}^1r, {}^2r) + {}^3r\,{}^2\phi({}^1r, {}^2r)$$

$$u_3({}^1r, {}^2r, {}^3r) = u_3({}^1r, {}^2r), \qquad {}^1\phi({}^1r, {}^2r) = \left\{u_{3,1} + \gamma_1({}^1r, {}^2r)\right\}$$

$${}^2\phi({}^1r, {}^2r) = \left\{u_{3,2} + \gamma_2({}^1r, {}^2r)\right\} \tag{2}$$

where ${}^1\phi({}^1r, {}^2r)$ and ${}^2\phi({}^1r, {}^2r)$ are the total rotations; $\gamma_1({}^1r, {}^2r)$ and $\gamma_2({}^1r, {}^2r)$ are the rotations due to shear deformation of the normal to the plate middle surface around the ${}^2\boldsymbol{g}$ axis and ${}^1\boldsymbol{g}$ axis, respectively, and $(),_i$ represents the partial differentiation of the variable preceding it with respect to ${}^ir$, the contravariant components of the position vector $\boldsymbol{r}$ $(\boldsymbol{r} = {}^1r\boldsymbol{g}_1 + {}^2r\boldsymbol{g}_2 + {}^3r\boldsymbol{g}_3)$.

The displacement fields are assumed as

$$u_1^0 = c_k({}^1r)^i({}^2r)^j, \qquad i, j = 0, 1, \quad k = 1, 4$$

$$u_2^0 = c_k({}^1r)^i({}^2r)^j, \qquad i, j = 0, 1, \quad k = 5, 8$$

$$u_3 = c_k({}^1r)^i({}^2r)^j + c_k({}^1r)^m({}^2r)^n + c_k({}^1r)^n({}^2r)^m$$

$$i, j = 0, 1, 2, 3, \quad m = 0, 1, \quad n = 4, 5, \quad k = 9, 32$$

$$\gamma_1 = c_k({}^1r)^i({}^2r)^j, \qquad i, j = 0, 1, \quad k = 33, 36$$

$$\gamma_2 = c_k({}^1r)^i({}^2r)^j, \qquad i, j = 0, 1, \quad k = 37, 40 \tag{3}$$

to match with 10 degrees of freedom $(u_1^0, u_2^0, u_3, u_{3,1}, u_{3,2}, u_{3,11}, u_{3,12}, u_{3,22}, \gamma_1,$ and $\gamma_2)$ per node in a four-noded element, where c_k are constants and are expressed in terms of nodal displacements. The 4×4 Gaussian quadrature scheme is adopted for computing the stiffness matrices and the load vector.

Now the covariant components of strain tensor ε $(\varepsilon = \varepsilon_{ij}{}^i\boldsymbol{g}{}^j\boldsymbol{g})$ can be written[18] in terms of displacement components $u(u = u_i{}^i\boldsymbol{g} = {}^k u\boldsymbol{g}_k)$ as

$$\varepsilon_{ij} = \tfrac{1}{2}\left(u_{i,j} + u_{j,i} + {}^k u_{,i} u_{k,j}\right) - \alpha_{ij} T \tag{4}$$

where α_{ij} $(\alpha_{13} = \alpha_{23} = 0)$ are thermal expansion coefficients. The normal strain component ε_{33} is zero. The strain energy of the plate can be written as

$$U = \frac{1}{2}\int_v \sigma^{ij}\varepsilon_{ij}\,\mathrm{d}v \tag{5}$$

where σ^{ij} are the contravariant components of stress tensor σ, that is, $\sigma = \sigma^{ij}\boldsymbol{g}_i\boldsymbol{g}_j$ and $\mathrm{d}v = \mathrm{d}^1r\,\mathrm{d}^2r\,\mathrm{d}^3r\cos\psi$.

The contravariant components of stress tensor σ^{ij} and the covariant components of the strain tensor ε_{ij} are related to their counterparts ${}^c\sigma_{mn}$ and ${}^c\varepsilon_{mn}$ and in the rectangular Cartesian coordinate system by

$${}^c\sigma_{mn} = \sigma^{ij}(\boldsymbol{g}_i \,.\, \boldsymbol{e}_m)(\boldsymbol{g}_j \,.\, \boldsymbol{e}_n) \tag{6}$$

$${}^c\varepsilon_{mn} = \varepsilon_{ij}\left({}^i\boldsymbol{g} \,.\, \boldsymbol{e}_m\right)\left({}^j\boldsymbol{g} \,.\, \boldsymbol{e}_n\right) \tag{7}$$

Now the stress–strain law in the rectangular Cartesian coordinate system can be written as

$${}^c\{\sigma_i\} = [Q_{ij}]^k\,{}^c\{\varepsilon_j\} \tag{8}$$

where ${}^c\{\sigma\} = \{\sigma_{11}\ \sigma_{22}\ \sigma_{13}\ \sigma_{23}\ \sigma_{12}\}^T$ and ${}^c\{\varepsilon\} = \{\varepsilon_{11}\ \varepsilon_{22}\ \varepsilon_{13}\ \varepsilon_{23}\ \varepsilon_{12}\}^T$ are Cartesian stress and strain components and $[Q_{ij}]^k$ represents plane stress reduced stiffness matrix of the kth laminate of the plate.

First-Ply Failure Analysis

In the present study, the following failure criteria are adopted to identify the material (first-ply) failure.[19,20]

Maximum Stress Criterion

Failure occurs if one of the following conditions is satisfied:

$$X_c > \sigma_1 > X_T, \qquad Y_c > \sigma_2 > Y_T, \qquad \sigma_{12} > R$$
$$\sigma_{13} > S, \qquad \sigma_{23} > T \tag{9}$$

where σ_1 and σ_2 are normal stress components; σ_{12}, σ_{13}, and σ_{23} are shear stress components; X_T and Y_T are the lamina strengths in the 1 and 2 directions, respectively; and R, S, and T are the shear strengths of the laminate in the 12, 13, and 23 planes, respectively.

Tsai–Hill Criterion

Failure occurs if the stresses satisfy the following single condition:

$$\left(\frac{\sigma_1}{X}\right)^2 + \left(\frac{\sigma_2}{Y}\right)^2 - \left(\frac{1}{X^2} + \frac{1}{Y^2} - \frac{1}{Z^2}\right)\sigma_1\sigma_2 + \left(\frac{\sigma_{12}}{R}\right)^2 + \left(\frac{\sigma_{13}}{S}\right)^2 + \left(\frac{\sigma_{23}}{T}\right)^2 \geq 1 \tag{10}$$

Tsai–Wu Criterion

In this case, the material failure is said to have occurred if the stresses satisfy the following condition:

$$F_1\,\sigma_1 + F_2\,\sigma_2 + 2F_{12}\,\sigma_1\,\sigma_2 + F_{11}\,\sigma_1^2 + F_{22}\,\sigma_2^2 + F_{44}\,\sigma_{13}^2 + F_{55}\,\sigma_{23}^2 + F_{66}\,\sigma_{12}^2 \geq 1 \tag{11}$$

where

$$F_1 = \frac{1}{X_T} - \frac{1}{X_C}, \qquad F_2 = \frac{1}{Y_T} - \frac{1}{Y_C}$$
$$F_{11} = \frac{1}{X_T X_C}, \qquad F_{22} = \frac{1}{Y_T Y_C}$$
$$F_{44} = \frac{1}{S^2}, \qquad F_{55} = \frac{1}{T^2}, \qquad F_{66} = \frac{1}{R^2}$$
$$F_{12} = -\frac{1}{2}\sqrt{\frac{1}{X_T X_C Y_T Y_C}}$$

Solution Procedure

The buckling load (temperature) calculation is carried out in two steps.[6–9,21] First, the prebuckling equilibrium equation

$$[K_s]\{\delta\} = \{F^T\} \tag{12}$$

is solved under the specified boundary condition, and the membrane forces are obtained. Here $\{F^T\}$ is the thermal load vector corresponding to unit temperature rise. Note that, in the present study of symmetrically laminated plates under uniform temperature rise, only membrane forces are generated. The geometric stiffness matrix $[K_{gm}]$ associated with this membrane forces is evaluated.[6,21] The critical buckling temperature (T_c) at which Euler-type buckling occurs is found from solving the following eigenvalue problem[6–9,21]:

$$\{[K_s] + \lambda_{cr}[K_{gm}]\}\{\delta\} = \{0\} \tag{13}$$

The lowest eigenvalue λ_{cr} is the critical buckling temperature. After buckling, the nonlinear equilibrium equation for plate problem under consideration may be expressed as[12]

$$\{([K_s] + [K_{nl}]) + \lambda[K_{gm}]\}\{\delta\} = \{0\} \tag{14}$$

Here, the force vector in the right-hand side is zero because the temperature effects (membrane forces) are accounted in the geometric stiffness matrix. The scalar multiplier λ, associated with geometric stiffness matrix, may be considered to represent the intensity of membrane forces due to temperature rise, that is, it represents the temperature load. Equation (14) is solved as an eigenvalue problem to get the temperature parameter λ when small displacement increments relative to the previous equilibrium state are considered to obtain the thermal postbuckling equilibrium path.[11,12] The detailed procedure is described here.

For a particular maximum out of plane displacement, say $0.02h$ (where h is the thickness of the plate) the buckling mode shape may be scaled up such that the maximum displacement component is $0.02h$ and the nonlinear stiffness matrix $[K_{nl}]$ may be formed. Now Eq. (14) is solved as an eigenvalue problem to obtain a new eigenvalue (temperature) and corresponding eigenvector (mode shape). The new eigenvector is scaled up again, and the maximum displacement component is held as $0.02h$. The nonlinear stiffness matrix is modified, and Eq. (14) is solved again to obtain a new eigenvalue and eigenvector. This procedure is repeated until the successive eigenvalues (λ, representing temperature) converge, that is, until the prescribed convergence criterion is satisfied. Similarly, the value of the maximum displacement may be increased to $0.04h$, $0.06h$, and so on, and the corresponding temperatures (eigenvalues) may be found.

The stresses are calculated, and different failure criteria are employed to identify the first-ply failure. After identifying the laminates, which have failed in strength, the stiffness matrix is modified accordingly and equilibrium iterations are carried out to locate the new equilibrium position of the plate.

A computer program was developed as per the aforementioned formulation, and it has been validated with the existing results available in the literature, the boundary conditions for which the results have been obtained are as follows:

1) In the simply supported (SS) case (SS boundary condition), $u_1 = u_2 = u_3 = 0$ along the boundary nodes.

2) In the clamped (CL) edge case (CL boundary condition), $u_1 = u_2 = u_3 = 0$, $u_{3,1} = 0$ at ${}^1r = 0, a$, and $u_1 = u_2 = u_3 = 0$, $u_{3,2} = 0$ at ${}^2r = 0, b$.

Results and Discussion

The critical buckling temperatures of an isotropic CL skew plate have been obtained with different mesh sizes to study the convergence of results. They are reported in Table 1. The results of Table 1 show that the convergence is monotonic and that the authors' results compare well with those of Prabhu and Durvasula.[16] Furthermore, the authors' results of the 6×6 mesh size are also acceptable when compared with those of higher mesh sizes and of Prabhu and Durvasula.[16] Hence, for further numerical work, a 6×6 mesh size has been adopted. The present formulation also performs well for the thick plate as seen from the results of Table 2 (Ref. 22). Moreover, the element yielded six nearly zero eigenvalues establishing it to be free from locking and any spurious zero energy mode. The comparison of the authors' results for the postbuckling paths with those of 1), Prabhu and Durvasula[16] in Fig. 2 of a isotropic clamped skew plate and 2), Singh et al.[11] in Fig. 3 of an SS square composite plate establishes the validation of the computer code developed.

Thereafter, the authors have taken up eight-layered Kevlar® 49/epoxy plates for both SS and CL boundary conditions with the

Table 1 Comparison of critical temperature parameter T^* for clamped isotropic skew plate; $T^* = E\alpha a^2 h T_{cr}/(\pi^2 D)$

Skew angle, deg	Mesh size				Prabhu and Durvasula[16]
	4×4	6×6	8×8	10×10	
0	3.64	3.69	3.70	3.71	3.71
15	3.87	3.92	3.93	3.94	3.95
30	4.73	4.76	4.78	4.79	4.80
45	6.86	6.87	6.89	6.90	6.92

Table 2 Comparison of nondimensionalized deflections[a] $\bar{w}$ in a three-layer, cross-ply $[0^0/90^0/0^0]$ SS square laminates under uniform loading q_0

a/h	Reddy[22]		Present element with 6×6 mesh size
	Higher-order shear deformation theory	First-order shear deformation theory	
100.0	0.6705	0.6697	0.6709
50.0	0.6838	0.6807	0.6824
20.0	0.7760	0.7573	0.7609
10.0	1.0900	1.0219	1.0322
4.0	2.9091	2.6596	2.7198

[a]Deflections $\bar{w} = (wE_2h^3 \times 10^2)/q_0a^4$, $E_1 = 174.6$ GPa, $E_2 = 7$ GPa, $G_{12} = G_{13} = 3.5$ GPa, $G_{23} = 1.4$ GPa, $\mu_{12} = \mu_{13} = 0.25$.

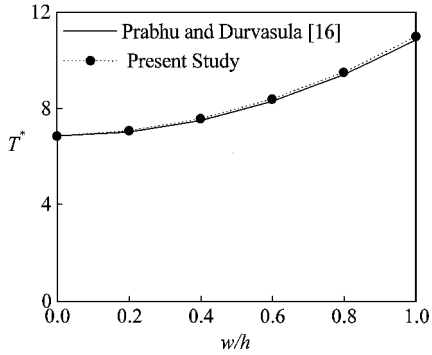

Fig. 2 Postbuckling equilibrium paths of isotropic CL skew (skew angle 45 deg) plate; temperature parameter $T^* = E\alpha a^2 h T_{cr}/\pi^2 D$, where T_{cr} is the buckling temperature ($a = b$) and w/h is maximum displacement.

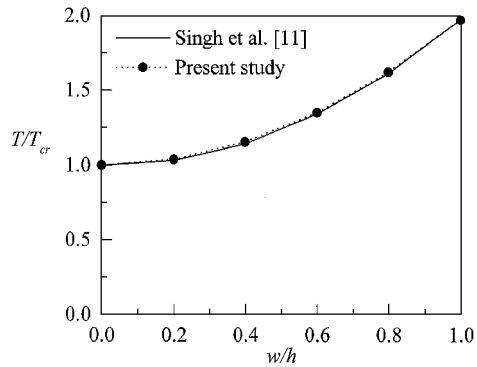

Fig. 3 Postbuckling paths of an SS four-layered angle-ply [45/− 45/45/− 45 deg] plate ($E_L/E_T = 40.0$, $G_{LT}/E_T = G_{LZ}/E_T = 0.5$, $G_{TZ}/E_T = 0.2$, $\mu_{LT} = 0.25$, $\alpha_T/\alpha_L = 10.0$).

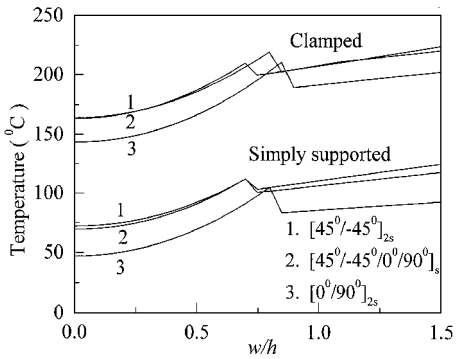

Fig. 4 Postbuckling paths of SS and CL composite skew plate (skew angle = 30 deg, $a = b$).

respective skew angles of 0, 30, and 45 deg. The material properties of the adopted Kevlar 49/epoxy laminates[23] are as follows: $E_L = 76\,\text{GPa}$, $E_T = 5\,\text{GPa}$, $G_{LT} = G_{LZ} = G_{TZ} = 2\,\text{GPa}$, $\mu_{12} = 0.34$, $\alpha_L = -4.0 \times 10^{-06}$, $\alpha_T = 79.0 \times 10^{-06}$, $X_t = 1379\,\text{MPa}$, $X_c = 276\,\text{MPa}$, $Y_t = 30\,\text{MPa}$, $Y_c = 138\,\text{MPa}$, and $R = S = T = 60\,\text{MPa}$.

Figure 4 presents a typical plot of temperature vs maximum displacement for three different symmetric layups of $[45/-45\text{ deg}]_{2s}$, $[45/-45/0/90\text{ deg}]_s$, and $[0/90\text{ deg}]_{2s}$ for a skew plate. The postbuckling paths have been obtained by solving Eq. (14) as a series of linear eigenvalue problems, as explained before, with maximum displacement as an independent variable. It is revealed from Fig. 4 that for the first and second layup, $[45/-45\text{ deg}]_{2s}$ and $[45/-45/0/90\text{ deg}]_s$, respectively, the buckling temperatures are higher and very close to each other. Moreover, the said composites maintain higher postbuckling resistance (temperature) from the buckling to the initiation of the secondary instability, that is, to the sudden decrease of postbuckling resistance, as explained later. Hereafter, several additional problems of thermomechanical buckling and postbuckling analyses of Kevlar 49/epoxy eight-layered $[45/-45/0/90\text{ deg}]_s$ laminated composite skew plates are taken up with SS and CL boundary conditions.

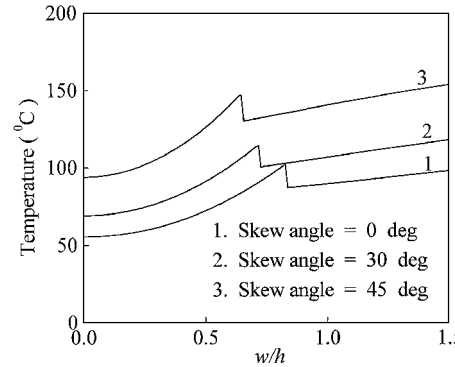

Fig. 5a Postbuckling paths of SS composite $[45/-45/0/90\text{ deg}]_s$ skew plate for different skew angle ($a = b$ and $a/h = 100.0$).

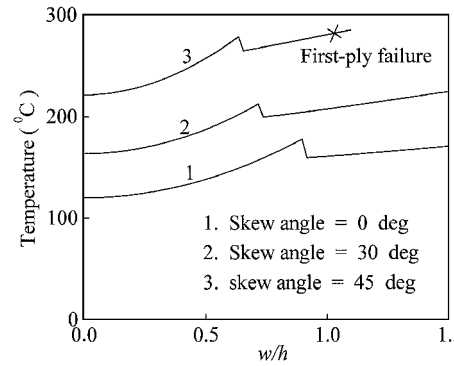

Fig. 5b Postbuckling paths of CL composite $[45/-45/0/90\text{ deg}]_s$ skew plate for different skew angle ($a = b$ and $a/h = 100.0$).

The variation of postbuckling temperatures (degrees Celsius) with maximum displacement has been presented in Figs. 5a and 5b for SS and CL composite skew plates, respectively, with different skew angles. It may be observed from Figs. 5a and 5b that the plate maximum displacement increases with the increase in temperature. Then, suddenly, the postbuckling resistance drops down and then again increases marginally with the increase in plate displacement. This sudden decrease of postbuckling resistance corresponds to the secondary instability. Moreover, the transition from primary postbuckling path to the secondary postbuckling path, that is, the near vertical line segments, are not statically stable. This secondary instability is observed for all of the cases, but its location is different for different skew angles of the plate as may be observed from Figs. 5a and 5b. However, when the skew angle is 45 deg, the CL plate fails after secondary instability at $w/h = 1.03$ due to excessive stress. This failure corresponds to the first-ply failure as identified by maximum stress criterion. Moreover, the buckling temperature and postbuckling paths for both SS and CL boundary conditions are always higher for the higher values of the skew angles. The secondary instability corresponds to the change in mode shape as can be seen in Figs. 6a and 6b, where the deflected shapes (mode shapes) of square SS and CL plates are plotted. From Figs. 6a and 6b, it is clear that the maximum out of plane displacement occurs at the center of the plate in the postbuckling regime. However, the location of maximum displacement shifts from center toward one side in the secondary instability regime.

The thermal load-displacement relations of the SS initially compressed laminated skew plates has been shown in Figs. 7a and 7b for skew angles of 30 and 45 deg, respectively, for different values of initial compressive load P. The initial compressive load P is expressed as a percentage of critical uniaxial mechanical buckling load. It may be observed from Figs. 7a and 7b that with the increase of initial compressive force P, the thermal buckling load and the postbuckling resistance decreases. Moreover, the secondary

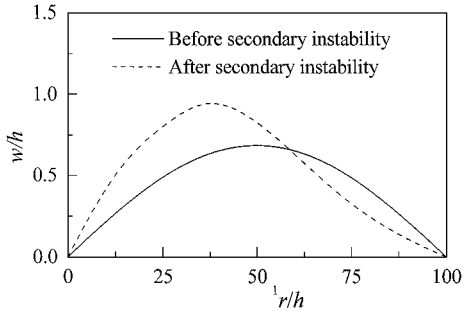

Fig. 6a Deflection shapes of SS square plate in postbuckling regime ($a = b$ and $a/h = 100.0$).

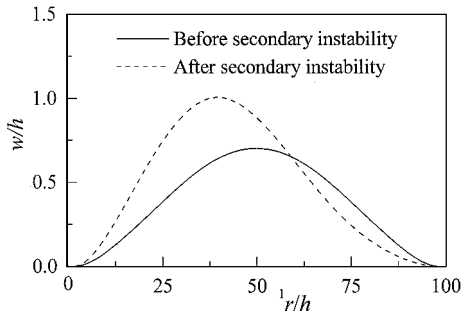

Fig. 6b Deflection shapes of CL square plate in postbuckling regime ($a = b$ and $a/h = 100.0$).

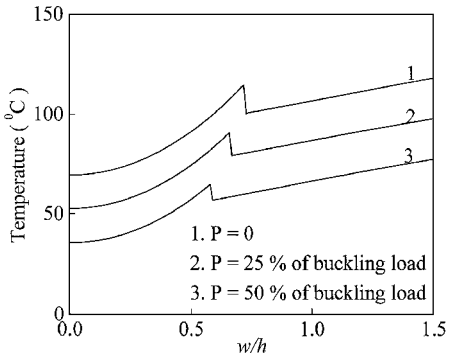

Fig. 7a Thermal postbuckling paths of initially compressed SS eight layered [45/– 45/0/90 deg]$_s$ skew plate for different initial compression P ($P = 0$, 25, and 50% of buckling load; $a/h = 100.0$; and skew angle = 30 deg).

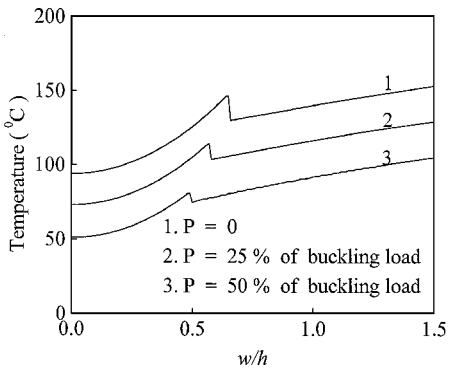

Fig. 7b Thermal postbuckling paths of initially compressed SS eight-layered [45/– 45/0/90 deg]$_s$ skew plate for different initial compression P ($P = 0$, 25, and 50% of buckling load; $a/h = 100.0$; and skew angle = 45 deg).

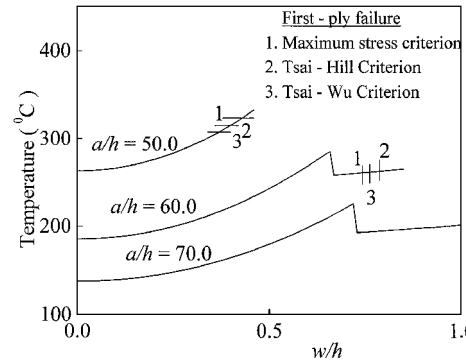

Fig. 8 Prediction of first-ply failure in thermal postbuckling paths of SS eight-layered [45/– 45/0/90 deg]$_s$ thick skew plate by different failure theories ($a/h = 50$, 60, and 70 and skew angle = 30 deg).

instability is observed at successively lower values of maximum transverse displacement with the increase of initial compressive force. A comparative study of Figs. 7a and 7b shows that both the buckling temperatures and the postbuckling paths are higher for the skew angle of 45 deg than those for the skew angle of 30 deg for each of the three initial compressive load cases taken up here.

Figure 8 shows the postbuckling temperatures and the first-ply failure load by different failure criteria of an SS thick skew (skew angle 30 deg) plate for different values of thickness-to-spanratios. From Fig. 8 it may be observed that the first-ply failure occurs in the postbucklingregime when the thickness-to-spanratio is 50.0. Maximum stress criterion gives the maximum failure temperature, and Tsai–Wu criterion gives the minimum failure temperature. The difference between the two failure predictions is about 6%. However, when the thickness-to-spanratio is 60.0, the first-ply failure occurs in the secondary instability regime, and the maximum stress criterion gives the minimum failure temperature, whereas the Tsai–Hill criterion gives the maximum failure temperature. Note that, when the thickness to span ratio is more than 70.0, secondary instability is predominant, and failure does not occur within $w/h = 1.0$.

Conclusions

The buckling and postbuckling analysis of shear-deformable composite skew plates subjected to combined uniaxial compression and uniform temperature rise has been carried out using the finite element method. The analysis reveals the presence of secondary instability, which branches out from the initial postbuckled path. The onset of secondary instability depends on the skew angle and initial compression. This can be identified by solving Eq. (12) as a series of linear eigenvalue problems for different amplitudes of lateral deflections. Different failure criteria, such as Tsai–Hill criterion and Tsai–Wu criterion in the stress space are used to predict the first-ply failure load and compared with the predictions of maximum strength criterion.

The authors' observations for the specific cases taken up in the present investigation clearly show the superiority of higher skew angles for both SS and CL boundary conditions. This conclusion is based on both buckling as well as postbuckling paths being higher when the skew angle is 45 deg.

References

[1]Gossard, M. L., Seide, P., and Roberts, W. M., "Thermal Buckling of Plates," NACA TN 2771, 1952.

[2]Klosner, J. M., and Forray, M. I., "Buckling of Simply Supported Plates Under Arbitrary Symmetrical Temperature Distribution," *Journal of the Aeronautical Sciences*, Vol. 25, No. 3, 1958, pp. 181–184.

[3]Gowda, R. M. S., and Pandalai, K. A. V., "Thermal Buckling of Orthotropic Plates," *Studies in Structural Mechanics*, edited by K. A. V. Pandalai, Indian Inst. of Technology, Madras, India, 1970, pp. 9–44.

[4]Meyers, C. A., and Hyer, M. W., "Thermal Buckling and Postbuckling of Symmetrically Laminated Composite Plates," *Journal of Thermal Stresses*, Vol. 14, No. 4, 1991, pp. 519–540.

[5]Whitney, J. M., and Ashton, J. E., "Effects of Environment on the Elastic Response of Layered Composite Plate," *AIAA Journal*, Vol. 9, No. 9, 1971, pp. 1708–1713.

[6]Thangaratnam, K. R., Palaninathan, R., and Ramachandran, J., "Thermal Buckling of Composite Laminated Plates," *Computers and Structures*, Vol. 32, No. 5, 1989, pp. 1117–1124.

[7]Prabhu, M. R., and Dhanaraj, R., "Thermal Buckling of Laminated Composite Plates," *Computers and Structures*, Vol. 53, No. 5, 1994, pp. 1193–1204.

[8]Lee, J., "Thermally Induced Buckling of Laminated Composites by a Layerwise Theory," *Computers and Structures*, Vol. 65, No. 6, 1997, pp. 917–922.

[9]Singha, M. K., Ramachandra, L. S., and Bandyopadhyay, J. N., "Optimum Design of Laminated Composite Plates for Maximum Thermal Buckling Loads," *Journal of Composite Material*, Vol. 34, No. 23, 2000, pp. 1982–1997.

[10]Huang, N. N., and Tauchert, T. R., "Large Deflection of Laminated Cylindrical and Doubly Curved Panels Under Thermal Loading," *Computer and Structures*, Vol. 41, No. 2, 1991, pp. 303–312.

[11]Singh, G., Rao, G. V., and Iyengar, N. G. R., "Thermal Postbuckling Behavior of Laminated Composite Plates," *AIAA Journal*, Vol. 32, No. 6, 1994, pp. 1336–1338.

[12]Chen, L. W., and Chen, L. Y., "Thermal Postbuckling Behaviors of Laminated Composite Plates with Temperature Dependent Properties," *Composite Structures*, Vol. 19, 1991, pp. 267–283.

[13]Shen, H. S., "Thermo-mechanical Postbuckling Analysis of Imperfect Laminated Plates Using a Higher Order Shear-Deformation Theory," *Computers and Structures*, Vol. 66, No. 4, 1998, pp. 395–409.

[14]Noor, A. K., and Burton, W. S., "Computational Models for High-Temperature Multilayered Composite Plates and Shells," *Applied Mechanics Reviews*, Vol. 45, No. 10, 1992, pp. 419–445.

[15]Prabhu, M. S. S., and Durvasula, S., "Thermal Buckling of Restrained Skew Plates," *Journal of Engineering Mechanics*, Vol. 100, No. 6, 1974, pp. 1292–1295.

[16]Prabhu, M. S. S., and Durvasula, S., "Thermal Post-Buckling Characteristics of Clamped Skew Plates," *Computers and Structures*, Vol. 6, No. 3, 1976, pp. 177–185.

[17]Pryor, C. W., Jr., and Barker, R. M., "Finite Element Analysis Including Transverse Shear Effects for Application to Laminated Plates," *AIAA Journal*, Vol. 9, No. 5, 1971, pp. 912–917.

[18]Liao, C. L., and Lee, Z. Y., "Elastic Stability of Skew Laminated Composite Plates Subjected to Biaxial Follower Forces," *International Journal of Numerical Methods in Engineering*, Vol. 36, No. 4, 1993, pp. 1825–1847.

[19]Engelstad, S. P., Reddy, J. N., and Knight, N. F., Jr., "Postbuckling Response and Failure Prediction of Graphite-Epoxy Plates Loaded in Compression," *AIAA Journal*, Vol. 30, No. 8, 1992, pp. 2106–2113.

[20]Kam, T. Y., and Sher, H. F., "Nonlinear and First-Ply Failure Analysis of Laminated Composite Cross-Ply Plates," *Journal of Composite Materials*, Vol. 29, No. 4, 1995, pp. 463–481.

[21]Cook, R. D., Malkus, D. S., and Plesha, M. E., *Concepts and Applications of Finite Element Analysis*, Wiley, New York, 1989, p. 442.

[22]Reddy, J. N., "A Simple Higher-Order Theory for Laminated Composite Plates," *Journal of Applied Mechanics*, Vol. 51, 1984, pp. 745–752.

[23]Phillip, L. N., *Design with Advanced Composite Materials*, edited by L. N. Phillip, Design Council, London, Springer-Verlag, Berlin, 1989, pp. 73–88.

E. R. Johnson
Associate Editor